

EUROPEAN COMMISSION – FCH JU

HORIZON 2020 PROGRAMME - TOPIC H2020-FCH-02-4-2019
New Anion Exchange Membrane Electrolysers

GRANT AGREEMENT No. 875024



Anion Exchange Membrane Electrolysis for
Renewable Hydrogen Production on a Wide-Scale

ANIONE – Deliverable Report

**D 4.1 Data set on catalytic activity, electrochemical performance and stability
of enhanced catalysts**



This project has received funding from the Fuel Cells and Hydrogen 2 Joint Undertaking (JU) under grant agreement No 875024. This Joint Undertaking receives support from the European Union's Horizon 2020 research and innovation programme, Hydrogen Europe and Hydrogen Europe research.



XRD Analysis

NiFe oxide-hydroxide Fresh

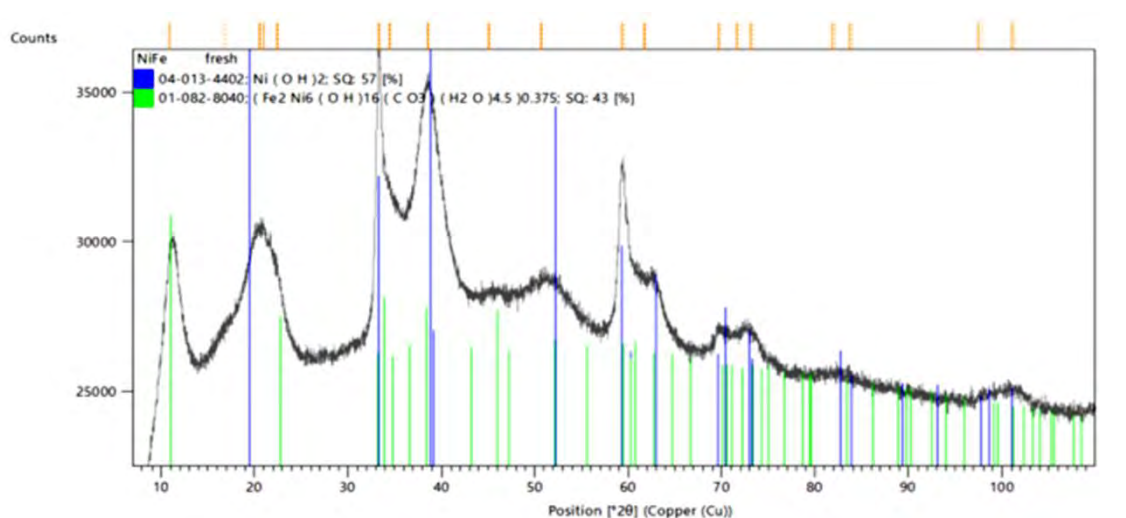


Figure 5. XRD pattern for NiFe oxide-hydroxide fresh sample. Correlating to reference patterns; Ni(OH)_2 (blue) and $\text{Fe}_2\text{Ni}_6(\text{OH})_{16}(\text{CO}_3)(\text{H}_2\text{O})_{4.5}$ (green).

XRD spectra of NiFe oxide-hydroxide fresh (Fig. 5) correlate to two structures, Ni(OH)_2 and $\text{Fe}_2\text{Ni}_6(\text{OH})_{16}(\text{CO}_3)(\text{H}_2\text{O})_{4.5}$. This material is showing broad peaks and narrower peaks, the result of a mixture of fine crystallite size and larger crystallite sizes with an average crystallite size of 27 Å (2.7 nm) calculated using the Scherrer formula. A slight positive shift in Ni(OH)_2 peaks implies a mixed metal hydroxide structure. Diffraction peaks corresponding to $\text{Fe}_2\text{Ni}_6(\text{OH})_{16}(\text{CO}_3)(\text{H}_2\text{O})_{4.5}$ exhibits general structural features of the typical signature for hexagonal lattices with $R3m$ rhombohedral symmetry. Although the chemical formula is different here, it has been confirmed these positions of the diffraction peaks in XRD patterns are almost the same for oxide-hydroxide with various divalent and trivalent metal ratios. [1][2] Semi-quantitative results are indicating nickel hydroxide and iron nickel hydroxide with an approximate 6 : 4 ratio.

NiFe oxide-hydroxide *Calcined*

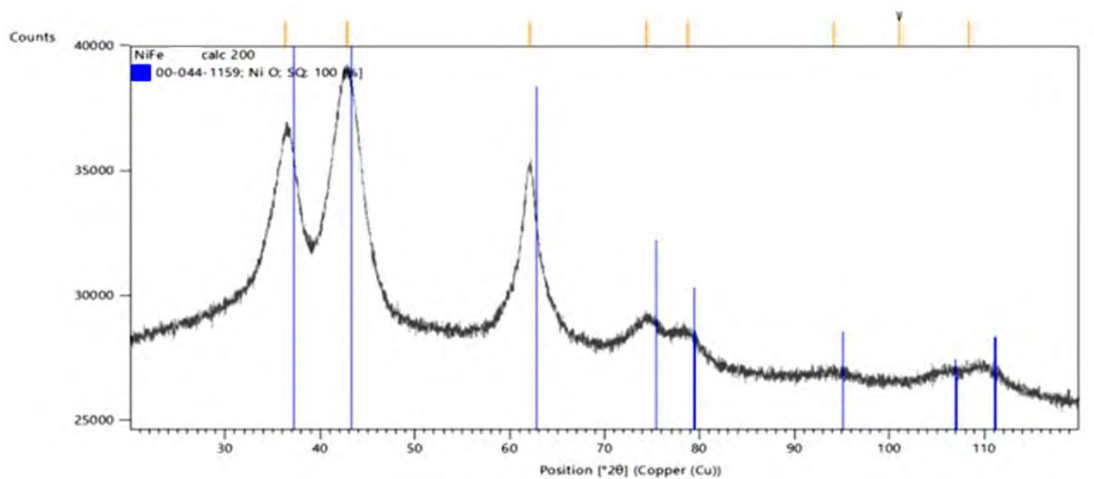


Figure 6. XRD pattern of NiFeOx calcined sample. Correlating to reference pattern NiO (blue).

Calcining NiFe oxide-hydroxide has a significant effect on the crystal structure of the material. The hydroxide precursor present in Figure , has been successfully oxidised, forming peaks correlating to NiO, $2\theta = 36, 43, 62, 74, 78^\circ$ as shown in Figure 6. However, all the peaks are significantly shifted from the positions for pure NiO, giving evidence for a mixed oxide of nickel and iron within the same crystal structure. Broad peaks and a crystallite size of 23 \AA (2.3 nm) is indicating a fine crystallite structure.

NiCu Reduced

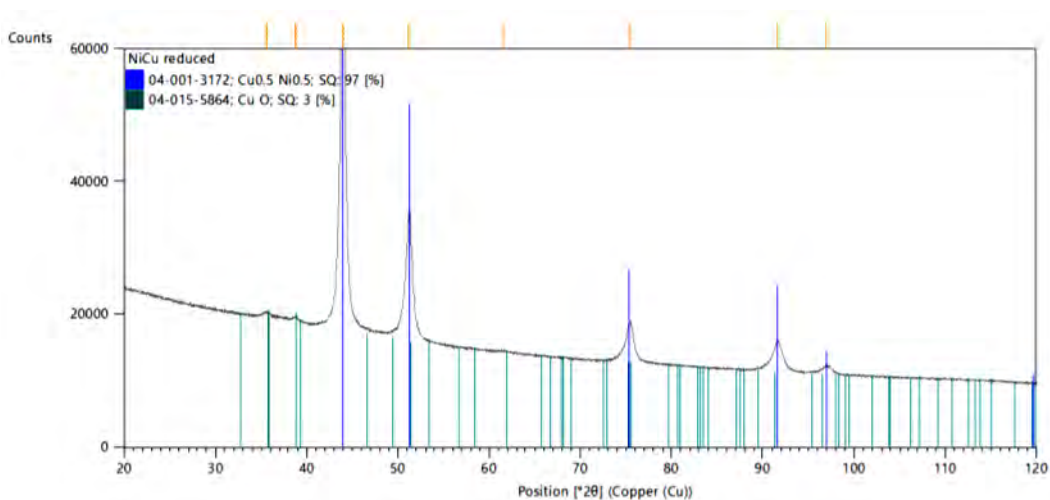


Figure 7. XRD pattern of NiCu reduced sample. Correlating to reference patterns; $\text{Cu}_{0.5}\text{Ni}_{0.5}$ (blue) and CuO (green).

The XRD pattern of NiCu, Figure 7, is revealing larger and narrow peak corresponding well with $\text{Cu}_{0.5}\text{Ni}_{0.5}$, at $2\theta = 44, 51, 75, 91.5$ and 97° . A large crystallite size of approximately 100 \AA is calculated. There are also a few minor peaks present, best matched with CuO albeit with a low intensity, semi-quantitative results reporting only 3%.

NiCuMo Reduced

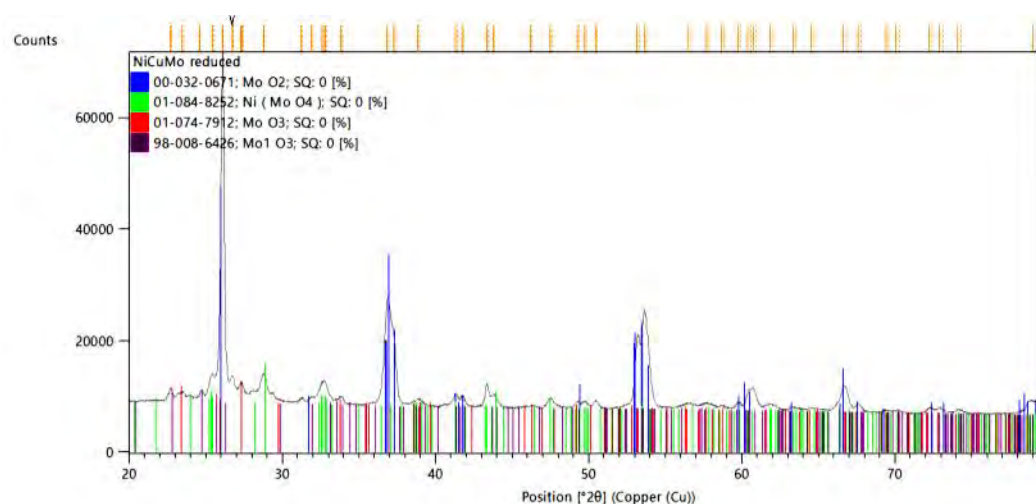


Figure 8. XRD pattern of NiCuMo reduced sample. Correlating to reference patterns; MoO_2 (blue), $\text{Ni}(\text{MoO}_4)$ (green), MoO_3 (red) and MoO_3 (black).

XRD pattern of reduced NiCuMo is presented in Figure 8. A large number of peaks, many of which at a low intensity creating a large number of possibilities in the Ni, Co, Mo and O system. Peaks at $2\theta = 26, 39.9, 37.2, 53, 53.5, 60$ and 67° directly correspond to MoO_3 . Numerous minor peaks corresponding to polymorphs of MoO_4 , and a mixed metal oxide, $\text{Ni}(\text{MoO}_4)$ and are detected, albeit a loose match at a low intensity. Interestingly, Ni and particularly Cu oxide structures are not detected. This may be due to one of two reasons; either Cu and Ni based

structures possess short range order or their expected ratio of 1:1:1 Cu : Ni : Mo is not their true values. This may be due to a leaching effect during the washing treatment.

SEM analysis

Typical SEM images of all 4 samples are shown in Figure 9, at 50 μm scale. Clearly shown is a variety of particle sizes and morphology across the 4 materials, typical oxide-hydroxide Nanosheet structure is not observed for any of these materials. NiFe oxide-hydroxide Fresh (top left) shows irregular sizes with a smooth surface of the particle, calcination of this sample has little effect on the morphology (top right). NiCu material (bottom left) shows smaller particle sizes ($<5 \mu\text{m}$), and more uniformity in size. This will lead to NiCu experiencing the highest surface area of all the four materials. NiCuMo exhibits a larger variety of particle size than NiCu. A mixture of finer particles, $<5 \mu\text{m}$ and larger particles, approximately 10 - 50 μm in size is observed. SEM images at a higher magnitude is shown in figure highlighting the smooth structure of NiFe particles, while NiCu based materials exhibit a much rougher surface, contributing to increased surface area.

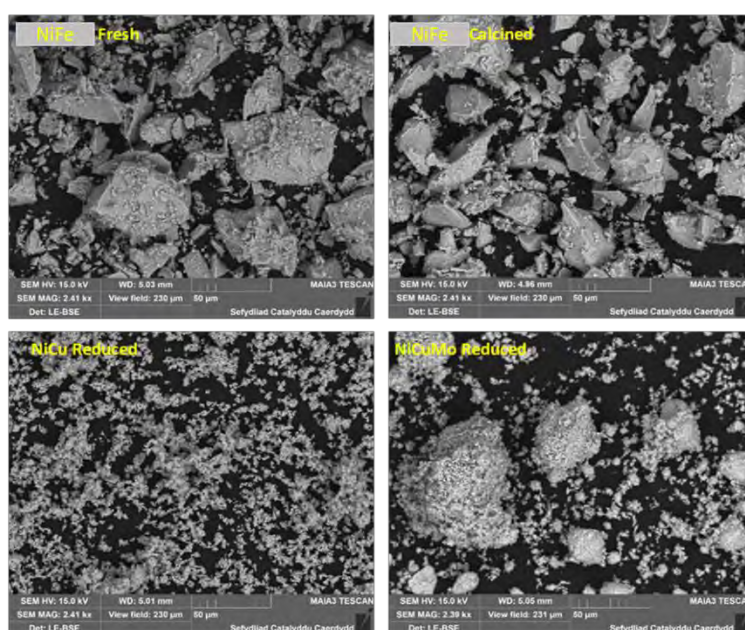


Figure 9. SEM images at low aof NiFe oxide-hydroxide Fresh (top left), NiFeOx Calcined (top right), NiCu Reduced (bottom left), NiCuMo Reduced (bottom right). Scale: 50 μm , Technique: LE-BSE.

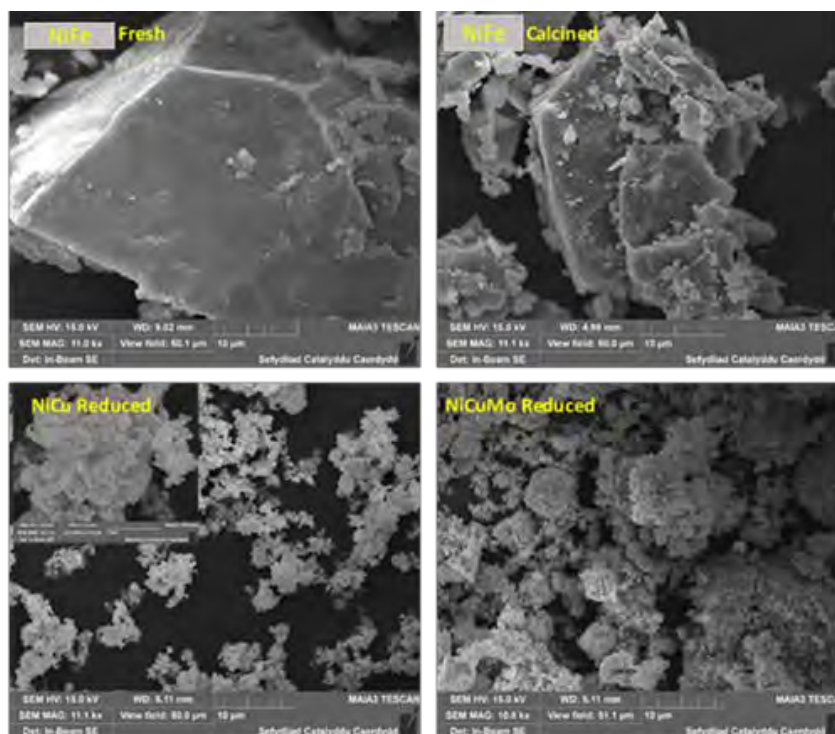


Figure 10. SEM images of NiFe oxide-hydroxide Fresh (top left), NiFeOx Calcined (top right), NiCu Reduced (bottom left), NiCuMo Reduced (bottom right). Scale: 10 μm , Technique: In-Beam SE.

EDS analysis

As shown in Figure 11, metal elements are uniformly distributed along all four materials, in accordance to SEM images. EDS analysis of NiFe composites gives a 5:1 molar ratio of Ni and Fe (Table 2), coinciding with the expected ratio. NiCu has an expected molar ratio of 1:1, correlating with a well defined XRD pattern of $\text{Ni}_{0.5}\text{Cu}_{0.5}$. EDS of NiCuMo exhibits a molar ratio of 1.5:1:7; here, molybdenum element exceeds the expected molar ratio 7-fold. This excess

of Mo is evident within XRD patterns, correlating to a majority of molybdenum oxide structures (Figure 11). Evidence to suggest that a large amount of Ni and Cu is not precipitated during the synthesis, and the metal precursors are washed away. Leaching studies during the synthesis may confirm this. The reducing conditions of both NiCu and NiCuMo exhibit a lower surface oxygen content, as opposed to fresh and calcined NiFe samples, as shown in Table 2. However, the oxygen content for NiCu is not as low as one would expect, implying a longer reduction treatment may be required.

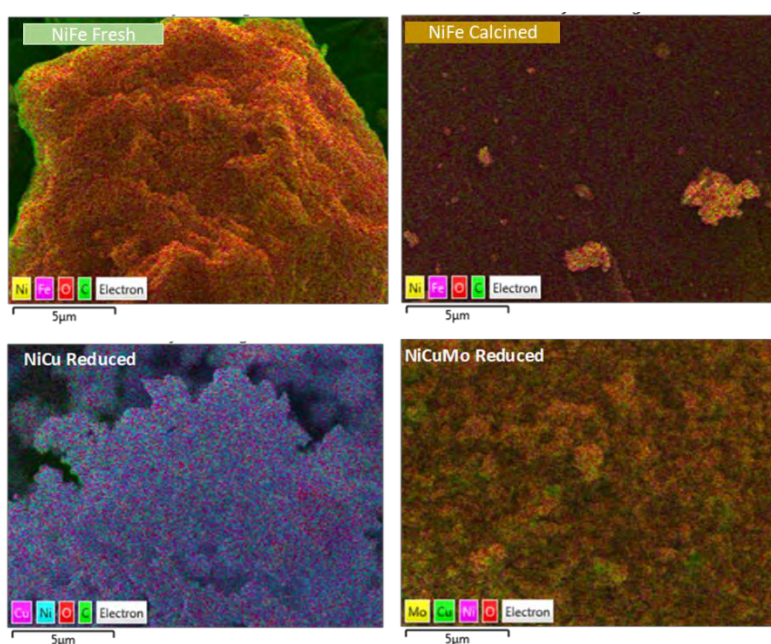


Figure 11. EDS analysis: SEM images of NiFe oxide-hydroxide Fresh (top left), NiFeOx Calcined (top right), NiCu Reduced (bottom left), NiCuMo Reduced (bottom right). Images showing distribution of Ni, Fe, Cu, Mo, O, C. Atomic percentages listed in Table 2.

Table 2. EDS quantitative results.

Catalyst	Expected Ratio	Surface At. %	Surface Ratio	O At. %

NiFe oxide- hydroxide Fresh	Ni:Fe 5.7 : 1	<i>Ni</i> 10.3 <i>Fe</i> 1.9	5.4 : 1	44.4
NiFeOx Calcined	Ni:Fe 5.7 : 1	<i>Ni</i> 11.5 <i>Fe</i> 2.2	5.2 : 1	31.1
NiCu Reduced	Ni:Cu 1 : 1	<i>Ni</i> 5.8 <i>Cu</i> 5.4	1 : 1	17.7
NiCuMo Reduced	NiCu:Mo 2 : 1	<i>Ni</i> 0.6 <i>Cu</i> 0.4 <i>Mo</i> 2.8	1.5 : 1 : 7	9.2

In summary, NiFe oxide-hydroxide anode materials and NiCu(Mo) cathode materials have been analysed by XRD, SEM and EDS. NiFe oxide-hydroxide precursor exhibited mixed metal hydroxides from XRD analysis, after which calcination formed a mixed metal oxide of good purity, possessing a small crystallite size. The likely reason for the promising performance of this anode in comparison to commercial catalyst (see below). SEM analysis shows a smooth surface with larger particles, and the expected Ni:Fe ratio is observed from EDS. NiCu(Mo) materials exhibited significantly larger crystallite sizes from XRD, corresponding with a poor cathodic performance. NiCu exhibits a well-defined $\text{Ni}_{0.5}\text{Cu}_{0.5}$ structure, however NiCuMo corresponds to dominantly molybdenum oxide, suggesting a deficiency of Ni and Cu within the material. This is supported by EDS, presenting a high molybdenum ratio in comparison to copper and nickel. SEM indicates NiCu(Mo) possesses smaller particle sizes resulting in an improved surface area in comparison to NiFe.

3.1.3 Electrochemical characterization of catalysts at CNR-ITAE

With regard to the electrochemical screening, because of the restricted access to the laboratories caused by the pandemic and related difficulties to purchase half-cell testing items, it was given priority to the in situ electrocatalysts assessment in single cell because this is considered more representative of the real operating conditions in the final stack prototype.

Slurries of the anode (NiFe oxide) and cathode (Pt/C as reference electrode for H₂ evolution acting as RHE, Ni, NiCu, NiCuMo as non critical raw materials) catalysts were prepared by dispersing the catalyst powder in ethanol in the presence of EM ionomer (the ionomer content in both anode and cathode catalyst layers was 33 wt.%). The cathode inks were deposited on carbon paper SIGRACET Gas Diffusion Layers (GDL) with a total metal loading of 3 mg cm⁻², the anodic ink was deposited on a Ni felt with 2.5 mg cm⁻² loading for NiFe. When Pt/C was used at the cathode (it is indicated in the specific figures), the catalyst loading was 1 mg Pt cm⁻². Pt/C was essentially used as reference electrode since it has the lowest overpotential for the hydrogen evolution reaction (HER). The process of H₂ evolution at Pt/C, thus, reproduces that of a reversible hydrogen electrode (RHE). A FAA3-50 anion exchange membrane in the OH⁻ form was used as separator between anode and cathode compartments. A cold-assembly procedure was assessed to prepare the membrane-electrode assemblies (MEAs) with 5 cm² geometrical area

The single cell was tested at different temperatures and under atmospheric pressure. The anode compartment was fed with a diluted KOH 1M solution at a flow rate of 4 mL min⁻¹ using a peristaltic pump. The KOH concentration is one order of magnitude less concentrated than in alkaline electrolysis. Polarization curves (cell potential as a function of current density) and chronopotentiometric curves were carried out with a Keithley power supply system (Tektronic). Electrochemical impedance spectroscopy (EIS) was carried out with a PGSTAT Autolab 302 Potentiostat/Galvanostat equipped with a booster of 20 A (Metrohm) and a Frequency Response Analyzer (FRA). EIS measurements were performed under potentiostatic control in a frequency range between 1 MHz and 10 mHz by frequency sweeping in a single sine mode and acquiring ten points per decade. The amplitude of the sinusoidal excitation signal was 0.01 V r.m.s.

3.1.4 Electrochemical characterization of Ni oxide anode catalyst at CNR-ITAE

Preliminary tests were carried out with a cell based on Pt/C as cathode and NiFe oxide as anode. Figures 12a-d show the impedance spectra collected at three potentials (i.e. 1.5 V, 1.8 V and 2 V) and at four different temperatures (i.e. 30 °C, 40 °C, 50 °C and 60°C).

All spectra exhibit at least 2 collapsed semicircles in which the high frequency semicircle is mainly due to the hydrogen evolution occurring on the Pt/C electrocatalyst and the low frequency semicircle is associated with the oxygen evolution occurring on the NiFe oxide electrocatalyst.

These figures show as the operating potential is affecting the semicircle appearing at low frequencies and it is a direct consequence of a larger overpotential shown by the NiFe oxide-based electrode.

In addition, the increased temperature reduced both the i) series resistances (i.e the intercept of spectra with x-axis at high frequencies) as a consequence of an enhanced conductivity of the membrane and the ii) total resistance (i.e. the intercept of spectra with x-axis at low frequencies) which is ascribed to better reactions kinetics.

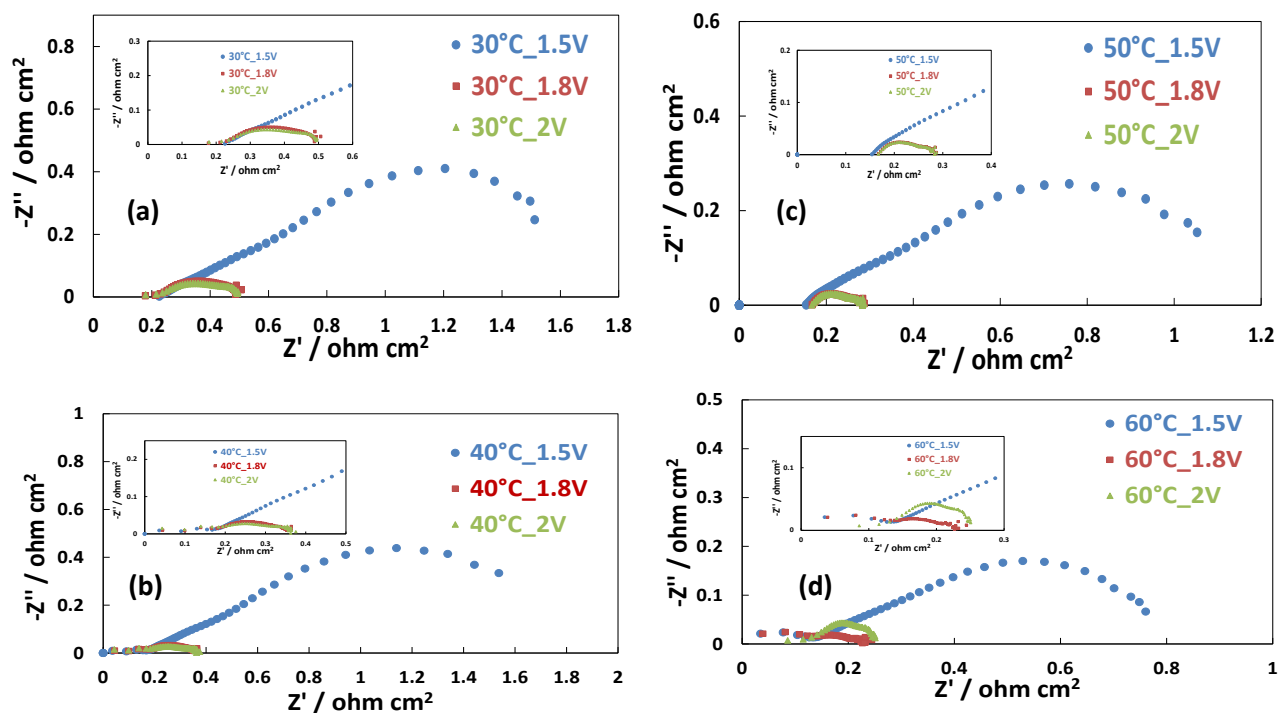


Figure 12. EIS carried out in the temperature range 30-60°C by feeding 1M KOH at the anode acquired at cell voltages of 1.5 V, 1.8 V and 2 V for the cell using Pt/C as cathode and NiFe oxide as anode.

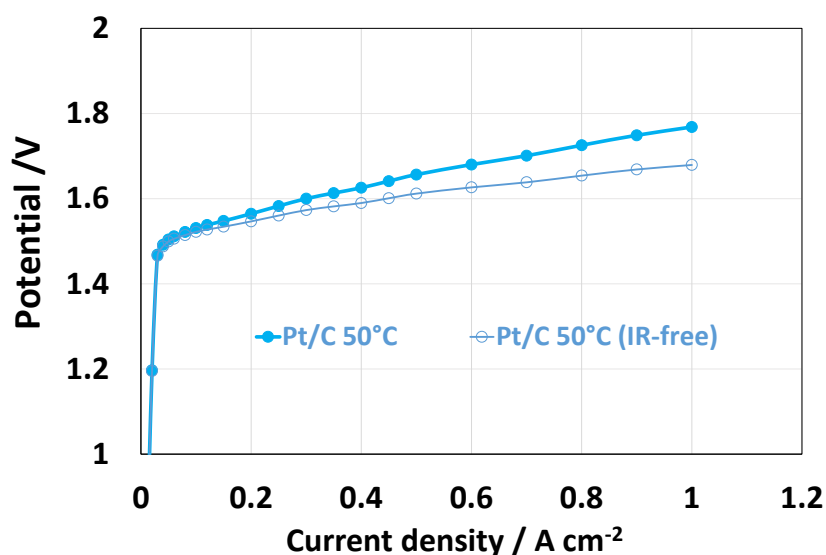


Figure 13. Polarisation curves carried out by feeding 1M KOH to the anode for the cell using Pt/C as cathode and NiFe oxide as anode.

Figure 13 shows the Polarisation curves carried out by feeding 1M KOH to the anode for the cell using Pt/C as cathode and NiFe oxide as anode indicating excellent performance of the anode in combination with a Pt cathode and a FAA-3 membrane.

Figure 14 shows the trend of anode overpotential vs. the current density evaluated for the cell based on Pt/C and NiFe oxide and investigated at 50 °C. This curve was calculated as following:

$$\eta_a = E_{Cell} - E_{cathode} - IR - E_{th} \quad (\text{eq. 1})$$

Where E_{cell} is the measured cell potential assumed as anode potential vs. RHE if $E_{cathode}$ is close to zero (small overpotential in the overall range of current density)

$$E_{anode} (IR - free) = E_{Cell} - E_{cathode} - IR \quad (\text{eq. 2})$$

$$\eta_a = E_{anode} (IR - free) - E_{th}$$

Here $E_{cathode}$ is assumed $E_{cathode}=0$ being the hydrogen evolution process over the reference Pt electrode almost reversible (RHE). E_{th} is the thermoneutral potential value of 1.48 V.

As observed in figure 14a, the activation control at the anode was 170 mV at 1 A cm⁻². The Tafel curve (i.e. anode overpotential vs. log. of current density) is shown in figure 14b. The Tafel slope is 118 mV/dec in the lowest current density range. This corresponds to a one electron transfer in the rate determining step. A larger slope at higher current densities may be indicative of mass transfer constraints.

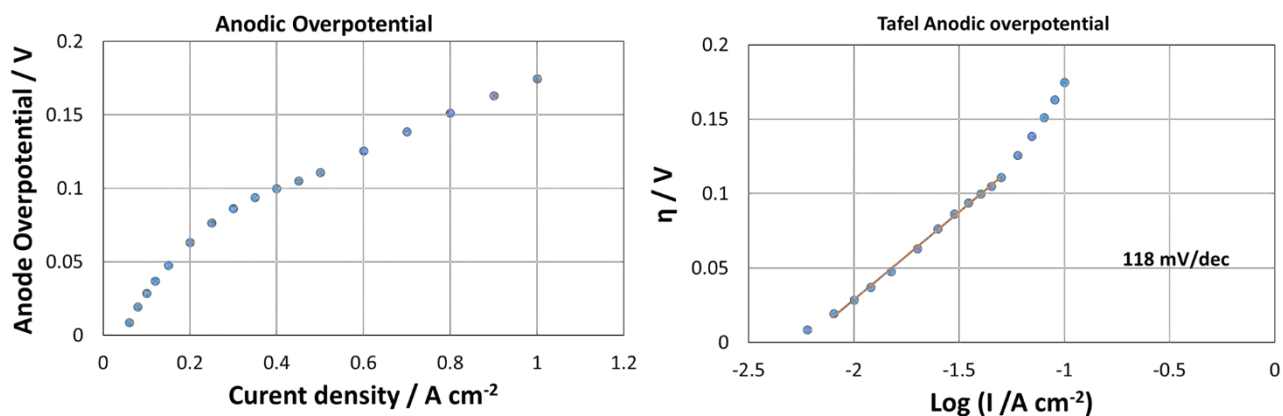


Figure 14. Anode overpotential of cell based on Pt/C as cathode and NiFe oxide as anode investigated at 50° determined according to eq. 1(a), and the Tafel slope (determined according to eq. 2 (b)).

Figure 15 reports the measure of cell voltage during a life-time test of about 1000 hrs under the galvanostatic operating conditions of 1 A cm⁻². During this test some interruptions occurred due to external factors e.g. laboratory issues etc. The cell potential rapidly increased in the first hours indicating the occurrence of recoverable losses (mass transfer issues); however, after a steady state was reached the successive behaviour shows continuous decrease of cell potential corresponding to an increase of cell efficiency. Test interruptions and replacement of the KOH solution resulted in a discontinuous behaviour. However, since the cell potential decreased with time no relevant degradation rate was observed in this time span.

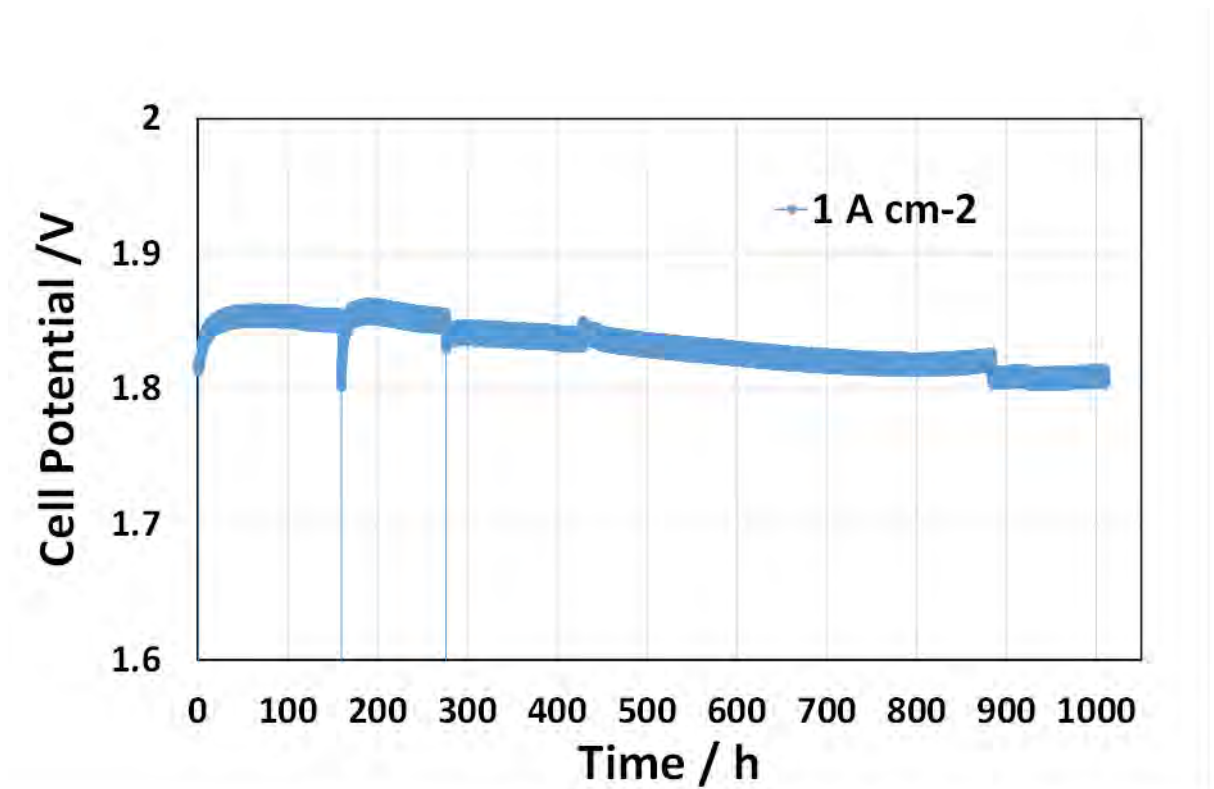


Figure 15. Life-time for the cell based on the NiFe oxide as anode and reference Pt cathode fed with 1M KOH at the anode and operating at 50 °C.

Figure 16 is related to the comparison of I-V curves collected at the beginning (BOL) and end (EOL) for this specific durability test and it shows that the performance of cell remains substantially identical without any relevant degradation, albeit the trend shown in the durability test was irregular and suffered from some interruptions (figure 15). Nevertheless, a slight improvement in performance was observed at the end of the test and it is essentially ascribed to a lower activation constraint probably associated with the anode reaction (i.e. oxygen evolution). No evidence of membrane degradation was observed since the ohmic slope remained the same after the prolonged test.

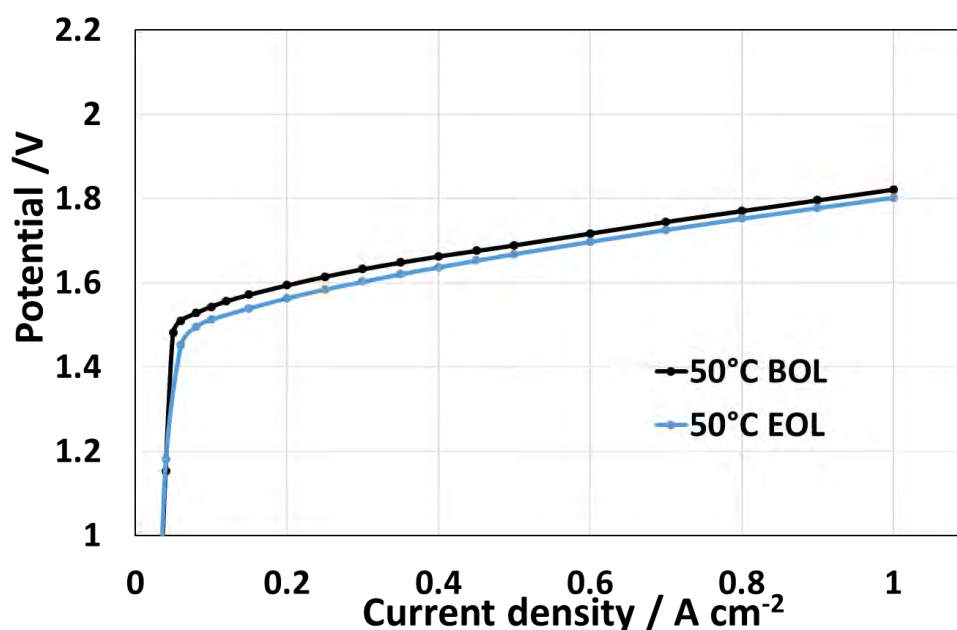


Figure 16. Comparison of polarisation curves at the beginning and end of the durability test carried out at 50 °C for the cell based on the NiFe oxide as anode and reference Pt cathode fed with 1M KOH at the anode.

The EIS analyses of figure 17 shows the different cell response before and after the prolonged test. The spectra consist of 2 semicircles. The semicircle at low frequency could be associated with the reaction characterised by the rate determining step (larger relaxation times) and this semicircle collapses with an increase in the cell voltage. The rate determining step in these experiments is related to the anodic process (i.e. oxygen evolution) being Pt used at the cathode. Moreover, after the durability test, the Impedance spectra showed that:

- i) the higher series resistance (R_s -intercept at high frequency with the x-axis) remained the same value indicating that the prolonged test did not affect the membrane conductivity, and
- ii) the semicircle appearing at low frequency of spectra collected at 1.5 V was much smaller

after prolonged test because of lower activation control for the oxygen evolution mechanism as shown in figure 17.

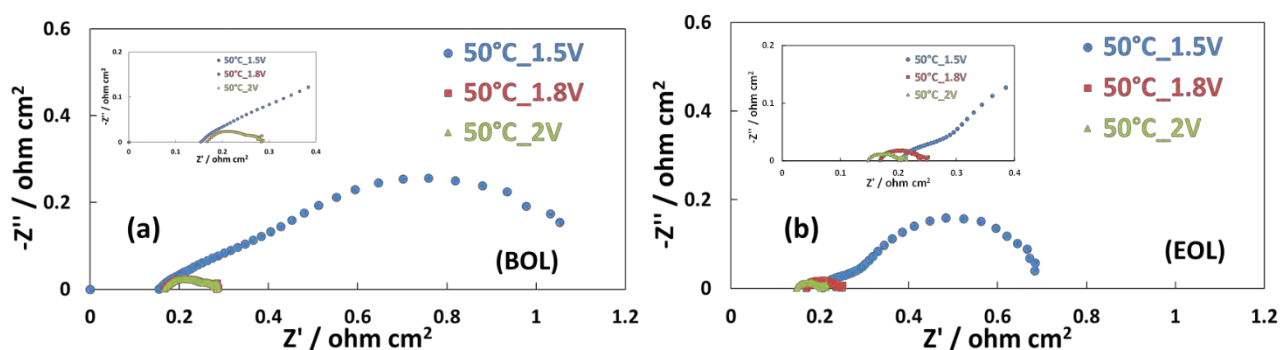


Figure 17. Comparison of EIS spectra carried out at 50 °C at the beginning and end of the durability test for the cell based on NiFe oxide anode and Pt/C as cathode.

3.1.4 Electrochemical characterization of Ni-based cathode catalysts at CNR-ITAE

The results discussed in this section refer to non CRM metallic Ni-based cathode catalysts cathodes developed at CNR- ITAE and assessed in single cell in the presence of NiFe Oxide anode. Since the anode potential of the NiFe Oxide was assessed against the RHE, this approach allow determining the cathode overpotentials for the metallic Ni –based catalysts.

A comparison of the non CRM Ni-based catalysts with the reference Pt cathode is presented.

In all experiments the same FAA3 membrane and the NiFe Oxide anode were used.

The preparation of specific slurries of these developed materials followed the above-mentioned preparation method for the Pt-based slurries to better compare their behaviours.

In figure 18, the polarisation curves carried out with reference cathode (Pt-based) and Ni are compared. As observed in the figure, the I-V curves of Ni conducted at 50 and 60 °C show a large activation control of about 400 mV compared to the curve of Pt. Only a slight mitigation of the activation control (about 20–30 mV) was observed as a consequence of the increased temperature. Figure 18 also includes the IR-free polarization curves (empty symbols). Here,

the effect of the increased temperature in the test conducted with the Ni-based cathode becomes noticeable, suggesting some ohmic constraint mainly referred to the electrolyte conductivity.

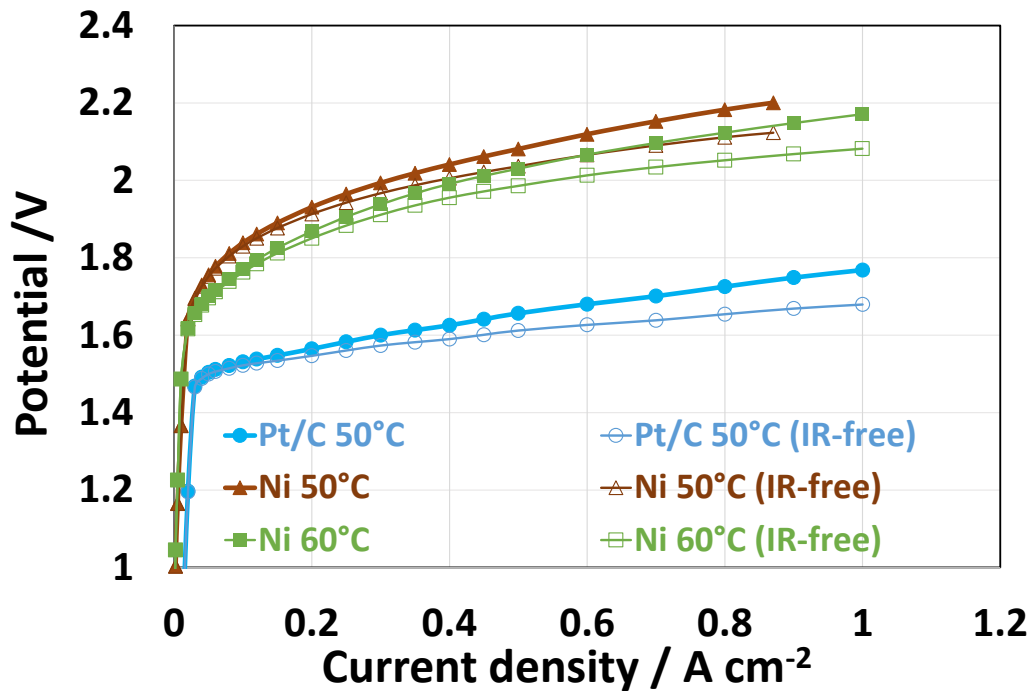


Figure 18. Polarization curves for Pt/C and metallic Ni cathodes measured at 50 and 60 °C by feeding 1M KOH feed to the anode based on NiFe oxide.

The successive figures show a comparison between a metallic NiCu-based electrocatalyst and Pt/C as cathode. In a preliminary test, the cell was investigated in the range of temperature 50–70 °C to individuate the most promising operating conditions. As observed in the Figure 19a, the NiCu showed a higher activation control compared to Pt. The activation loss was approximately 140 mV at the same temperature. Thus, significantly lower than that observed for pure Ni catalysts. An increase in the temperature reduced the overpotential of approximately 100 mV at 70 °C. Similar trends were observed for the IR-free curves (figure

19b). This underlines the differences in performance between Pt-based cathode and the non CRM cathode based on NiCu in terms of different activation losses caused by NiCu and Pt.

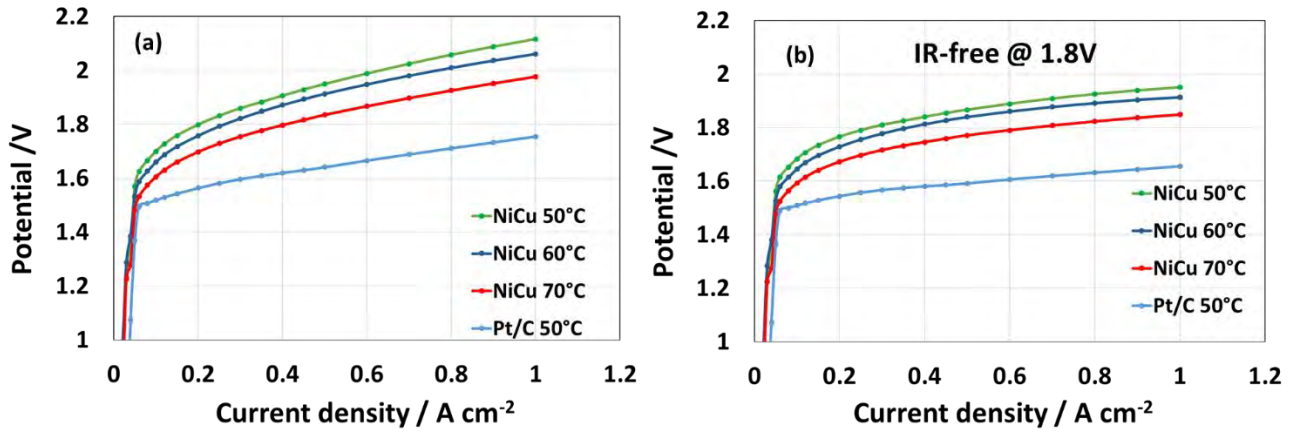


Figure 19. Polarization curves of Pt/C and NiCu measured in the temperature range 50-70°C by feeding 1M KOH feed to the anode based on NiFe oxide. Experimental I-V curves (a), experimental IR-free curves (b).

Figure 20a shows the trend of cathode overpotential vs. the current density evaluated for the experiment carried out at 70 °C and calculated as following:

$$\eta_c = E_{Cell} - IR - E_{th} - \eta_a \tag{eq. 3}$$

Where η_a is the anodic overpotential already determined for the NiFe oxide anode, the other terms have been defined above.

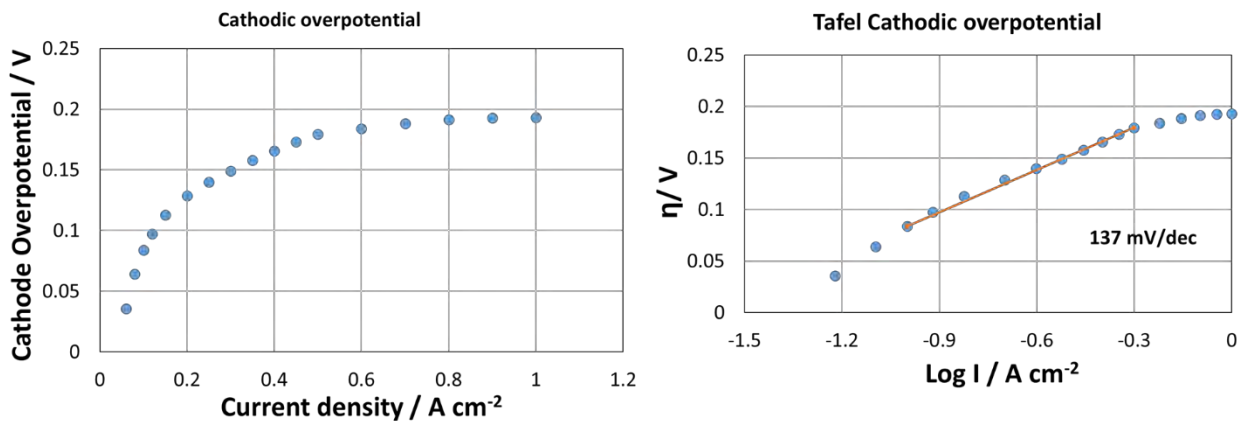


Figure 20. Cathode overpotential for NiCu as cathode at 70 °C, and related Tafel slope.

At 1 A cm^{-2} , the cathode overpotential is about 190 mV vs. the 150 mV project target. The Tafel slope of 137 mV /dec indicates a one-electron transfer reaction. The activation step appears thus related to the formation of hydrogen bonds (adsorption step) that is a slower process on Ni compared to Pt. Interestingly, the Tafel slope decreases significantly at high current densities possibly suggesting a shift to a $2e^-$ transfer reaction mechanism as r.d.s.

Beside these aspects, the larger overpotential of NiCu compared to Pt can be also related to the larger particles size (7 nm vs. 3 nm) corresponding to a lower active surface area.

Figures 21a and 22b show a comparison of EIS spectra collected in the temperature range 50–70 °C and at two potentials (i.e. 1.5 V and 1.8 V) for the cell based on Nicu cathode and NiFe oxide anode.

At 1.5 V, a large semicircle ascribed to the cathodic reaction is observed incorporating the semicircle of the anodic reaction.

Such behaviour is a direct consequence of high activation control of the cathodic reaction and is strictly connected with the low current density circulating in the cell at 1.5 V, albeit the increase temperature had an effective role in mitigating the activation losses. In fact, the dimension of the semicircles appearing at low frequency was strongly affected temperature.

Two well-defined semicircle were observed with the smaller semicircle appearing at lower frequencies (lower relaxation times).

An improved conductivity for the membrane is observed with increased temperature with a shift of R_s to lower values.